THE JOURNAL OF PHYSICAL CHEMISTRY A

ARTICLE

pubs.acs.org/JPCA

Density Functional and Spin−Orbit Ab Initio Study of CF_3Br: Molecular Properties and Electronic Curve Crossing

Joonghan Kim,[†] Tae Kyu Kim,[*,‡] and Hyotcherl Ihee[*,†]

[†]Center for Time-Resolved Diffraction, Department of Chemistry, Graduate School of Nanoscience & Technology (WCU), KAIST, Daejeon 305-701, Republic of Korea

[‡]Department of Chemistry and Chemistry Institute of Functional Materials, Pusan National University, Busan 609-735, Republic of Korea

Supporting Information

ABSTRACT: Quantum chemical calculations of CF_3Br and the CF_3 radical are performed using density functional theory (DFT) and time-dependent DFT (TDDFT). Molecular structures, vibrational frequencies, dipole moment, bond dissociation energy, and vertical excitation energies of CF_3Br are calculated and compared with available experimental results. The performance of six hybrid and five hybrid meta functionals in DFT and TDDFT calculations are evaluated. The ωB97X, B3PW91, and M05-2X functionals give very good results for molecular structures, vibrational frequencies, and vertical excitation energies, respectively. The ωB97X functional calculates well the dipole moment of CF_3Br. B3LYP, one of the most widely used functionals, does not perform well for calculations of the C—Br bond length, bond dissociation energy, and vertical excitation energies. Potential energy curves of the low-lying excited states of CF_3Br are obtained using the multiconfigurational spin−orbit ab initio method. The crossing point between $2A_1$ and 3E states is located near the C—Br bond length of 2.45 Å. Comparison with CH_3Br shows that fluorination does not alter the location of the crossing point. The relation between the calculated potential energy curves and recent experimental result is briefly discussed.

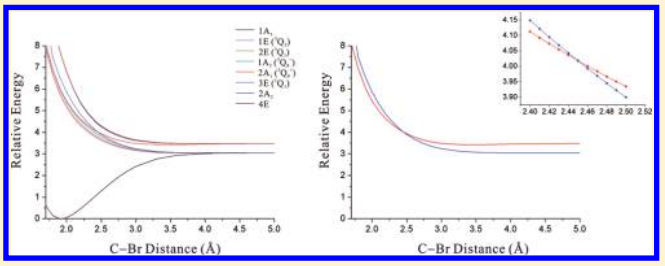

1. INTRODUCTION

Recent theoretical[1−7] and experimental[8−19] work has investigated the photodissociation dynamics of organic molecules with C—X (X = Br and I) bonds that can be broken by ultraviolet (UV) radiation. Most studies have focused particularly on the curve-crossing mechanism for the formation of X atoms in ground X ($^2P_{3/2}$) and excited X* ($^2P_{1/2}$) spin−orbit (SO) states.[2,3,7,12,13,18] The A-band photodissociation of CF_3Br is characterized by diffuse UV absorption continua of three repulsive states ($^1Q_1$ (3E), $^3Q_0$ ($2A_1$), and $^3Q_1$(2E)), which originate from n → σ* transitions localized in the C—Br bond that result in prompt dissociation. Detailed dynamics of state-selective photodissociation and nonadiabatic interaction of potential energy surfaces (PESs) have been elucidated from energy distributions, recoil anisotropy parameters, and the relative quantum yields of nascent Br atoms.[12,13,18]

In previous studies of the A-band photodissociation of CF_3Br, quantum yields of excited and ground SO states were explained in terms of nonadiabatic effects which arise from the reduction of symmetry of the parent molecule during dissociation.[12,13,18] As symmetry is reduced from C_{3v} to C_s, degenerate 3E and 2E states split into 5A′, 4A″, and 3A′, 2A″, respectively, and the $2A_1$ state corresponds to the 4A′ state. States 4A′ and 5A′ can interact to form an avoided crossing responsible for nonadiabatic dynamics following A-band excitation in C_s symmetry. Nonadiabatic crossing can be enhanced by the reduction of vibrational symmetry. Nonadiabatic effects depend on whether the parent molecule is initially pumped in the 3E or $2A_1$ state.[12,13,18] Experimental study of CF_3Br photodissociation indicates that the internal energy partitioning and branching ratio depend on the initially excited low-lying electronic states.[12,13,18] In a recent SO ab initio investigation of the photodissociation of CH_3I and CF_3I,[1−3] nonadiabatic crossing was explained in terms of the shape of the potential energy curves (PECs) and the electronic energy at the crossing point. Elucidating the photodissociation dynamics of CF_3Br is important as comparing results from CF_3Br with those from CH_3I and CF_3I can provide insight into the electronic and mass effects of substitutions, respectively. However, calculated results of CF_3Br have been lacking.

The most important geometric parameter of halomethanes and haloethanes is C—X distance. Because these molecules' PECs of low-lying excited states are strongly repulsive, their vertical excitation energies (T_v) are sensitive to the ground-state C—X bond length. Therefore, accurate calculation of the ground-state C—X distance is required to obtain accurate T_v values. Although halomethanes and haloethanes have been well

Received: October 1, 2010
Revised: December 25, 2010
Published: January 27, 2011

Table 1. Optimized Molecular Structures (C_{3v}; bond lengths/Å and bond angles/°) and Vibrational Frequencies (/cm^{-1}) of the CF_3 Radical by Ab Initio and DFT Calculations

CF_3 radical	HF	MP2	CCSD(T)	B3LYP	B3PW91	PBE0	mPW1PW91	exp.
r(C—F)	1.290	1.313	1.314	1.319	1.314	1.310	1.310	1.318 ± 0.002[a]
∠(F—C—F)	111.41	111.32	111.30	111.39	111.43	111.41	111.43	110.76 ± 0.4[a]
E	562	516	514	504	508	514	514	510[b]
A_1	772	717	712	698	704	712	711	701[b]
A_1	1215	1116	1108	1076	1091	1106	1105	1090[b]
E	1419	1280	1285	1235	1261	1285	1282	1260[b]
	B97-2	ωB97X	B1B95	TPSSh	BMK	M05-2X	M06-2X	exp.
r(C—F)	1.313	1.315	1.309	1.322	1.307	1.312	1.309	1.318 ± 0.002[a]
∠(F—C—F)	111.38	111.29	111.33	111.19	111.28	111.40	111.26	110.76 ± 0.4[a]
E	511	510	512	496	524	519	521	510[b]
A_1	708	706	710	690	722	712	716	701[b]
A_1	1092	1100	1106	1073	1138	1113	1123	1090[b]
E	1264	1272	1284	1226	1316	1297	1313	1260[b]

[a] Infrared spectroscopy data, ref 55. [b] Reference 56.

investigated using density functional theory (DFT) due to its fast computation time compared with ab initio methods, assessment of the C—X distance by DFT has still been lacking. Moreover, although time-dependent DFT (TDDFT) has been widely used to calculate T_v, the assessment of exchange−correlation functionals for TDDFT calculations of halomethanes and haloethanes have rarely been reported. Performance tests of TDDFT calculations of halomethanes may aid the development of new DFT functionals that can accurately predict T_v and advance further experimental photodynamic study of halomethanes and haloethanes.

In this work, DFT functionals for the molecular structures, vibrational frequencies, dipole moment, and bond dissociation energy (BDE) of CF_3Br are assessed. The performance of TDDFT in calculating T_v is also evaluated. Low-lying excited PECs are calculated using the multiconfigurational SO ab initio method. The crossing point, important for determining the branching ratio, is examined through one-dimensional PECs, and the relation between calculation and experiment is briefly discussed.

2. COMPUTATIONAL DETAILS

Geometry optimizations and subsequent vibrational frequency calculations were performed using DFT and ab initio methods. In the DFT calculations, we used six hybrid (B3LYP,[20,21] B3PW91,[22] PBE0,[23] mPW1PW91,[24,25] B97-2,[26] and ωB97X (long-range corrected)[27]) and five hybrid meta functionals (B1B95,[20,28] TPSSh,[29] BMK,[30] M05-2X,[31] and M06-2X[32]). Ab initio calculations employed Hartree−Fock (HF), Møller−Plesset second-order perturbation theory (MP2),[33,34] and coupled-cluster singles and doubles including perturbative corrections for the triple excitations (CCSD(T))[35] to compare results with those from DFT calculations. For C and F, the 6-311+G(3df) basis set was used. The scalar relativistic effect of Br was treated using the aug-cc-pVTZ-PP relativistic effective core potential (RECP).[36] TDDFT[37−39] was used to calculate T_v values of the spin-free states (^{1}E, ^{3}E, and $^3A_1$ states in C_{3v} symmetry) of CF_3Br. Configuration interaction singles (CIS)[40] and equation-of-motion CCSD (EOM-CCSD)[41] were also used to compare T_v values with those calculated by TDDFT. Basis set superposition error (BSSE) was corrected using the counterpoise (CP) method.[42] All of the above calculations were performed using the Gaussian09 program.[43]

The complete active space self-consistent field (CASSCF)[44] method was used to calculate the ground and low-lying excited states' PECs in CF_3Br. Six active electrons were distributed in six active orbitals, which included the σ-bonding orbital of C—Br, two nonbonding orbitals (n), and the σ* antibonding orbital of C—Br, in this method, hereafter labeled CAS(6,6). The active orbitals for CAS(6,6) calculations are shown in Figure S1 in the Supporting Information. The 6-311+G(3df) basis sets were used for C and F atoms. For Br, the 6-311G(3df) all-electron basis set with additional diffuse functions (s: α = 0.045593; p: α = 0.035142; d: α = 0.104700; f: α = 0.258000) of the aug-cc-pVTZ was used. Scalar relativistic effects were considered using the Douglas−Kroll−Hess second-order method (DKH2).[45,46] Six spin-free states were calculated using state-averaged CASSCF, $^1A_1$, ^{1}E, ^{3}E, and $^3A_1$ in C_{3v} symmetry. However, those electronic states were calculated using C_1 symmetry. Subsequently, spin−orbit multiconfigurational quasi-degenerate perturbation theory (SO-MCQDPT)[47] was used to obtain electronic states including spin−orbit coupling (SOC). Twelve SO coupled states were obtained. All electrons of CF_3Br were correlated in the MCQDPT2 calculations. The full Breit−Pauli Hamiltonian was used for the spin-dependent Hamiltonian. All CASSCF and SO-MCQDPT calculations were carried out using GAMESS code.[48] Table S1 in the Supporting Information summarizes for comparison each of the methods' performance in calculating various molecular properties.

3. RESULTS AND DISCUSSION

Molecular Structures. Parameters of the optimized molecular structures of the CF_3 radical and CF_3Br are summarized in Tables 1 and 2, respectively. To visualize the performance of tested methods, mean absolute errors (MAEs) calculated by including all bond lengths of CF_3Br and the CF_3 radical are shown in Figure 1a. MAEs of bond angles are not shown because all methods calculated them reasonably, producing similar values. Percentage errors of the C—Br bond length compared with experimental values have been estimated; their results are summarized in Figure 1b. Figure 1a shows that geometrical parameters calculated by HF deviated greatly from experimental values. The deviation of CAS(6,6) is more significant than that of

Table 2. Optimized Molecular Structures (C_{3v}; bond lengths/Å and bond angles/°), Vibrational Frequencies (/cm^{-1}), Dipole Moment (/Debye), and Bond Dissociation Energy (D_0 at 0 K/kcal mol^{-1}) of CF_3Br by Ab Initio and DFT Calculations

CF_3Br	HF (CAS(6,6))	MP2	CCSD(T)	B3LYP	B3PW91	PBE0	mPW1PW91	exp.
r(C—F)	1.297 (1.296)	1.324	1.324	1.327	1.323	1.319	1.319	1.3265(23)[a]
r(C—Br)	1.919 (1.953)	1.907	1.918	1.950	1.937	1.930	1.931	1.9234(31)[a]
∠(F—C—F)	108.74 (109.0)	108.63	108.61	108.76	108.81	108.81	108.81	108.81(25)[a]
∠(Br—C—F)	110.20 (109.9)	110.30	110.32	110.17	110.12	110.12	110.13	
ν_6(E)	334	312	308	297	301	304	304	297[b]
ν_3(A_1)	383	365	358	336	344	352	350	350,[b] 348[c]
ν_5(E)	606	555	553	543	548	553	553	548[b]
ν_2(A_1)	844	773	768	754	764	773	773	764,[b] 761[c]
ν_1(A_1)	1210	1105	1109	1060	1076	1094	1092	1087,[b] 1085[c]
ν_4(E)	1379	1222	1233	1184	1209	1232	1229	1206[b]
μ	0.518 (0.509)	0.788	0.838	0.543	0.464	0.457	0.476	0.639(2)[a]
D_0(CF_3—Br),[e,f] 0 K	*37.6*, *36.6*	*77.7*, *71.7*, **74.7**	*73.2*, *67.4*, **70.3**	*65.6*, *64.9*	*67.9*, *67.0*	*69.8*, *69.0*	*68.3*, *67.4*	70.1 ± 0.3[d]
	B97-2	ωB97X	B1B95	TPSSh	BMK	M05-2X	M06-2X	exp.
r(C—F)	1.321	1.324	1.318	1.329	1.316	1.321	1.318	1.3265(23)[a]
r(C—Br)	1.935	1.919	1.925	1.942	1.936	1.927	1.930	1.9234(31)[a]
∠(F—C—F)	108.81	108.56	108.73	108.72	108.68	108.74	108.71	108.81(25)[a]
∠(Br—C—F)	110.12	110.37	110.20	110.22	110.25	110.19	110.22	
ν_6(E)	303	306	301	292	308	312	310	297[b]
ν_3(A_1)	345	362	351	335	362	359	359	350,[b] 348[c]
ν_5(E)	551	551	551	535	563	560	559	548[b]
ν_2(A_1)	768	774	772	746	791	782	784	764,[b] 761[c]
ν_1(A_1)	1081	1112	1097	1052	1133	1109	1119	1087,[b] 1085[c]
ν_4(E)	1217	1221	1233	1179	1268	1246	1264	1206[b]
μ	0.444	0.655	0.535	0.464	0.673	0.589	0.584	0.639(2)[a]
D_0(CF_3—Br),[e,f] 0 K	*69.8*, *68.8*	*69.3*, *68.5*	*70.1*, *69.3*	*67.4*, *66.5*	*68.7*, *67.9*	*71.5*, *70.5*	*68.9*, *67.9*	70.1 ± 0.3[d]

[a] Microwave spectra data, ref 57. [b] Reference 58. [c] Reference 59. [d] Reference 60. [e] Values in italic are BSSE-corrected values using the CP method. [f] Values in bold are 50% of the BSSE-corrected values using the CP method.

HF because CAS(6,6) significantly overestimates the C—Br bond length. Such overestimation can be attributed to the small portion of the configuration where electrons occupy the σ^* (C—Br) orbital in the CAS(6,6) wave function; the electronic structure of CF_3Br involves 93.3%$(\sigma_{C-Br})^2(n_{Br})^2(n_{Br})^2(\sigma^*_{C-Br})$ and 4.8%$(\sigma_{C-Br})(n_{Br})^2(n_{Br})^2(\sigma^*_{C-Br})^2$ electronic configuration. In particular, only HF and CAS(6,6), which do not include dynamic electron correlation, give much shorter C—F bond lengths than experimentally observed (see Tables 1 and 2). This indicates that dynamic electron correlation is important to the accurate calculation of the C—F bond length. The C—Br distance calculated using HF is in good agreement with the experimental value, but this is accidental considering the absence of dynamic correlation in HF. MP2 underestimates the C—Br distance compared with the experimental value (see Table 2). The distance calculated by CCSD(T) is much closer to the experimental value than that of MP2. CCSD(T) reasonably describes the molecular structure of CF_3Br, with all of the geometric parameters calculated by CCSD(T) in good agreement with the experimental values (see Figure 1a). Most DFT methods overestimate the C—Br distance compared with the experimental value (see Table 2). Of the DFT methods, B1B95 provides the best result of the C—Br distance. Both M05-2X and ωB97X also give reasonable C—Br distances. All geometric parameters of CF_3Br calculated by ωB97X are in excellent agreement with those from CCSD(T). This result is surprising given previous work that showed that all DFT functionals (ωB97X was not used in the previous work) greatly overestimated the C−I distances of CF_2ICF_2I and the CF_2CF_2I radical.[6] To test the performance of ωB97X for larger molecules, such as haloethanes, the molecular structure of the anti structure of CF_2ICF_2I was optimized using ωB97X. The C−I distance was optimized at 2.148 Å, very reasonable compared to the results from CASPT2 (2.146 Å)[6] and from experiment (2.136 ± 0.007 Å).[49] Therefore, we can conclude that the ωB97X functional is adequate for predicting C—X (X = Br and I) distances. B3LYP seriously overestimates the C—Br distance (see Table 2 and Figure 1b). It similarly overestimates C−I distances in CF_2ICF_2I and the CF_2CF_2I radical.[6] Therefore, B3LYP is not appropriate for the calculation of C—X bond lengths. TPSSh also overestimates the C—Br bond length, making it also inadequate for the prediction of halomethanes' molecular structures. The hybrid meta functionals, except TPSSh, generally provide shorter C—Br distances compared with those calculated by the hybrid functionals. According to these results, we summarize the trend of description of the molecular structure of CF_3Br by ab initio and DFT calculations. Because MP2 overestimates the strength of the C—Br bond, its length is underestimated compared with the experimental value. Evidence of such an overestimation by MP2 can also be identified through the BDE results of the C—Br bond (see the BDE subsection and Table 2). In contrast, most DFT methods overestimate the C—Br bond length. The C—Br bond length calculated by CCSD(T) lies between that of MP2 and most DFT values. The molecular structure of CF_3Br appears

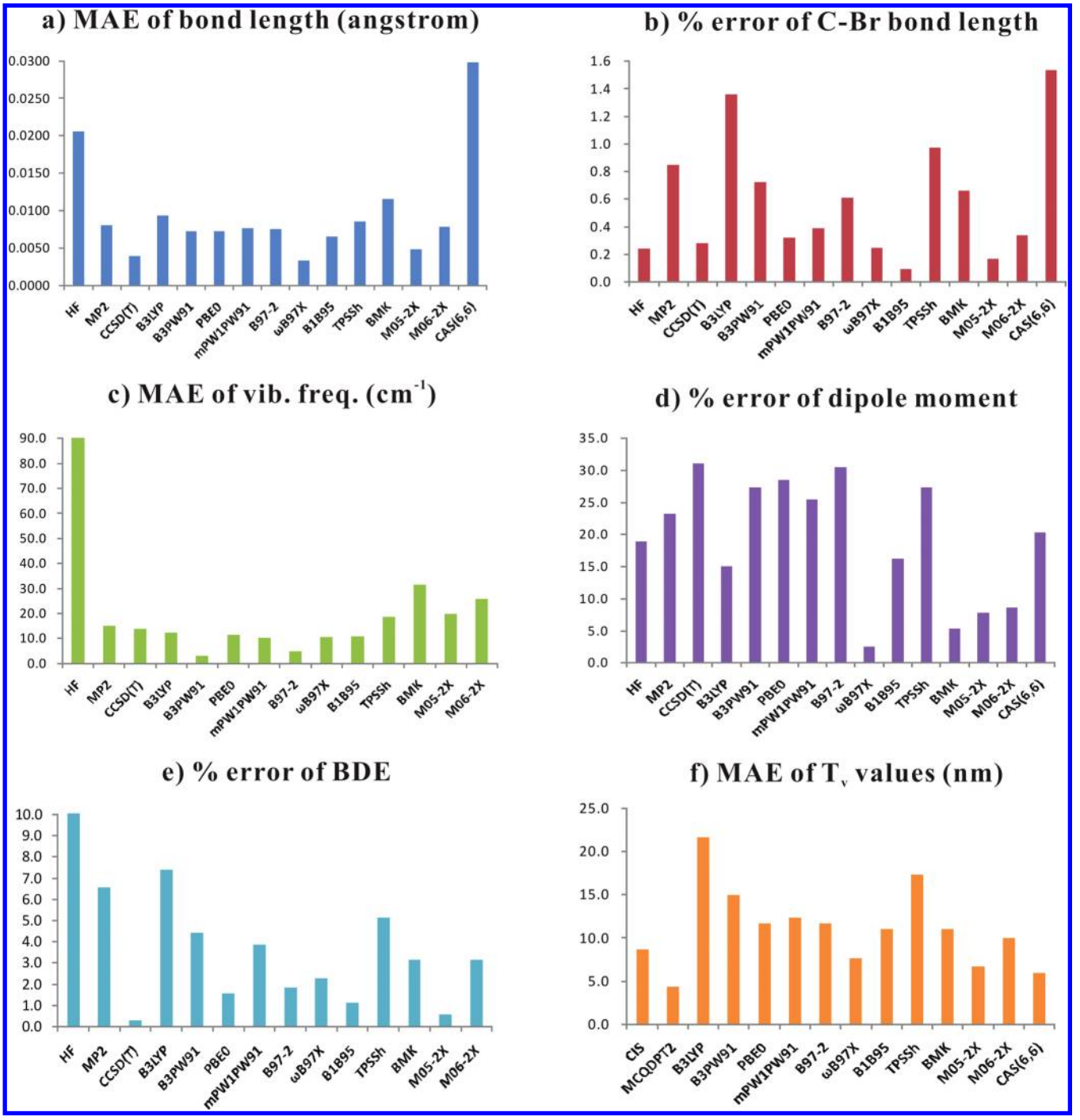

Figure 1. (a) MAE of the bond length (including the C—F bond length of the CF_3 radical), (b) percentage error of the C—Br bond length, (c) MAE of vibrational frequencies (including vibrational frequencies of the CF_3 radical), (d) percentage error of the dipole moment, (e) percentage error of BDE, and (f) MAE of T_v values.

best calculated by CCSD(T) (see Figure 1a). However, its computational cost is quite expensive, increasing the attractiveness of DFT methods. The choice of DFT functional is crucial to the determination of the molecular structure of CF_3Br. In this regard, ωB97X is strongly recommended, but the most popular DFT functional, B3LYP, should not be used for calculations of the molecular structures of halomethanes and haloethanes.

Vibrational Frequencies. Calculated vibrational frequencies of the CF_3 radical and CF_3Br are summarized in Tables 1 and 2, respectively. Their MAEs are also estimated (Figure 1c). HF greatly overestimated vibrational frequencies due to the absence of dynamic electron correlations (Tables 1 and 2 and Figure 1c). MP2 improves predictions of vibrational frequencies, and CCSD(T) gives results slightly closer to the experimental values. B3PW91 provides excellent results for the vibrational frequencies (see Figure 1c), with B97-2 also giving good results. Vibrational frequencies calculated by the hybrid meta functionals, except B1B95, substantially deviate from the experimental values. The recently proposed hybrid meta functionals BMK, M05-2X, and M06-2X tend to overestimate the vibrational frequencies of the

dx.doi.org/10.1021/jp109456v |J. Phys. Chem. A 2011, 115, 1264–1271

Table 3. Vertical Excitation Energies (T_v/nm) of Spin-Free States of CF_3Br by Ab Initio and TDDFT Calculations[a]

CF_3Br	CIS	EOM-CCSD	MCQDPT2 (CAS(6,6))	B3LYP	B3PW91	PBE0	mPW1PW91
^3E	203(206)	210	214(203)	238(227)	230(224)	226(223)	227(224)
^1E	172(174)	188	193(181)	207(198)	199(195)	195(193)	196(193)
$^3A_1$	163(163)	160	164(164)	178(169)	174(169)	172(169)	172(169)
	B97-2	ωB97X	B1B95	TPSSh	BMK	M05-2X	M06-2X
^3E	225(220)	222	224(223)	231(223)	224(219)	217(214)	221(218)
^1E	198(194)	194	197(196)	200(193)	195(192)	195(193)	199(197)
$^3A_1$	170(166)	165	170(168)	179(173)	172(168)	166(164)	168(165)

[a] Values in parentheses are T_v values calculated from the geometry optimized using CCSD(T).

CF_3 radical and CF_3Br. The hybrid functionals generally provide better results than the hybrid meta functionals in these vibrational frequency calculations. The ωB97X functional, which provides excellent results for the molecular structures, performs worse than B3PW91. DFT functionals B3PW91 and B97-2 are superior to high-level ab initio methods such as CCSD(T) for the calculation of vibrational frequencies.

Dipole Moment. The calculated dipole moments of CF_3Br are summarized in Table 2, with percentage errors shown in Figure 1d. HF underestimates, while MP2 and CCSD(T) overestimate the dipole moment of CF_3Br compared with the experimental value. All DFT methods, except ωB97X and BMK, underestimate the dipole moment. The ωB97X functional gives the best result, which is very close to the experimental value. BMK also performs reasonably. DFT methods are superior to the ab initio methods, but the selection of optimal functional, such as ωB97X, is important.

BDE. C—Br BDE calculations are summarized in Table 2, with percentages errors shown in Figure 1e. HF greatly underestimates BDE because of its lack of dynamic electron correlation. MP2 substantially overestimates the BDE of CF_3Br, while CCSD(T) slightly overestimates it. However, with BSSE correction, MP2 gives a result closer to the experimental value than CCSD(T) (see italic values in Table 2). Because overcorrection by the CP method in ab initio calculations is well-known,[50] the actual BDE calculated by CCSD(T) may be much closer to the experimental value. For example, the BDE by CCSD(T) with 50% BSSE correction[51] is 70.3 kcal/mol, in excellent agreement with the experimental value (70.1 $\pm$ 0.3 kcal/mol). However, MP2 with 50% BSSE correction gives 74.7 kcal/mol, larger than the experimental value, implying that MP2 overestimates the strength of the C—Br bond. Among the DFT methods, M05-2X provides the best result, which is in excellent agreement with the experimental observation (see Figure 1e). B1B95 also gives a reasonable result for the BDE of CF_3Br. All DFT methods underestimate BDE. In particular, B3LYP is the worst. TPSSh also greatly underestimates the BDE. It should be noted that once an appropriate DFT functional is selected to calculate BDE, it can provide accurate and cost-effective results.

Vertical Excitation Energy (T_v). The T_v values calculated by ab initio and TDDFT methods are summarized in Table 3. Their estimated MAEs for CF_3Br are shown in Figure 1f. We assume that EOM-CCSD gives the most accurate T_v, and thus, all MAEs are calculated by comparison with T_v values from EOM-CCSD. Both ^3E and ^1E states have n (nonbonding orbital of Br) $\rightarrow \sigma^*$ (antibonding orbital of C—Br) excitation character, while the $^3A_1$ state has σ (bonding orbital of C—Br) $\rightarrow \sigma^*$ (antibonding orbital of C—Br) excitation character. All TDDFT methods give red-shifted T_v values compared with those of EOM-CCSD (see Table 3). Especially B3LYP gives the most red-shifted T_v values. Of the DFT methods, M05-2X gives the closest values to those of EOM-CCSD (see Figure 1f). MCQDPT2 agrees well with EOM-CCSD. In contrast to other methods, CIS gives blue-shifted T_v values of the ^3E and the ^1E states (see Table 3). The degree of red shift of T_v values is closely related to the overestimation of the C—Br bond length (see Tables 2 and 3). Because B3LYP gives the longest C—Br distance (1.950 Å), T_v values calculated by TD-B3LYP are substantially red-shifted. The M05-2X functional, which gives a relatively short C—Br distance (1.927 Å), produces reasonable T_v values, closer to those of EOM-CCSD and MCQDPT2. A scatter plot of percentage errors of the C—Br bond length (x-axis, the results in Figure 1b) versus MAEs of T_v values (y-axis, the results in Table 3) is shown in Figure S2 of the Supporting Information. This plot shows a strong positive correlation coefficient (0.909), indicating that the accurate calculation of the C—Br distance is important for obtaining reasonable T_v values. In order to check only exchange−correlation dependence in TDDFT calculations, T_v values were calculated for the optimized geometry by CCSD(T) (see values in parentheses in Table 3). This method can provide reasonable geometric parameters with respect to the experimental parameters (see Figure 1a). Because ωB97X gives a very similar optimized geometry to CCSD(T), TD-ωB97X calculation using the geometry optimized by CCSD(T) was not performed. TDDFT results based on the geometry optimized by CCDS(T) give closer values to those of EOM-CCSD and MCQDPT2 compared with results based on geometries optimized by each method. However, with the exceptions of M05-2X and M06-2X, discrepancies between T_v values of EOM-CCSD and those from DFT are still large. The T_v values calculated by M05-2X on the CCSD(T) geometry perfectly match those of MCQDPT2 and are very close to those of EOM-CCSD. According to these results, M05-2X provides reasonable results for the T_v values of CF_3Br, which is also shown in a previous investigation of CF_2ICF_2I.[6] In summary, to obtain accurate T_v values, the correct choice of exchange−correlation functionals for TDDFT calculations as well as reasonable C—Br distances is crucial.

Potential Energy Curves (PECs). Several low-lying excited-state PECs were calculated by SO-MCQDPT, and the PECs are shown in Figure 2. In the calculation, the 6 spin-free states ($^1A_1$, ^1E, ^3E, and $^3A_1$ in C_{3v} symmetry) are mixed by SOC, generating 12 SO coupled states. The minimum point of the C—Br bond length for the ground state in the SO-MCQDPT calculation is 1.920 Å, in excellent agreement with the experimental value

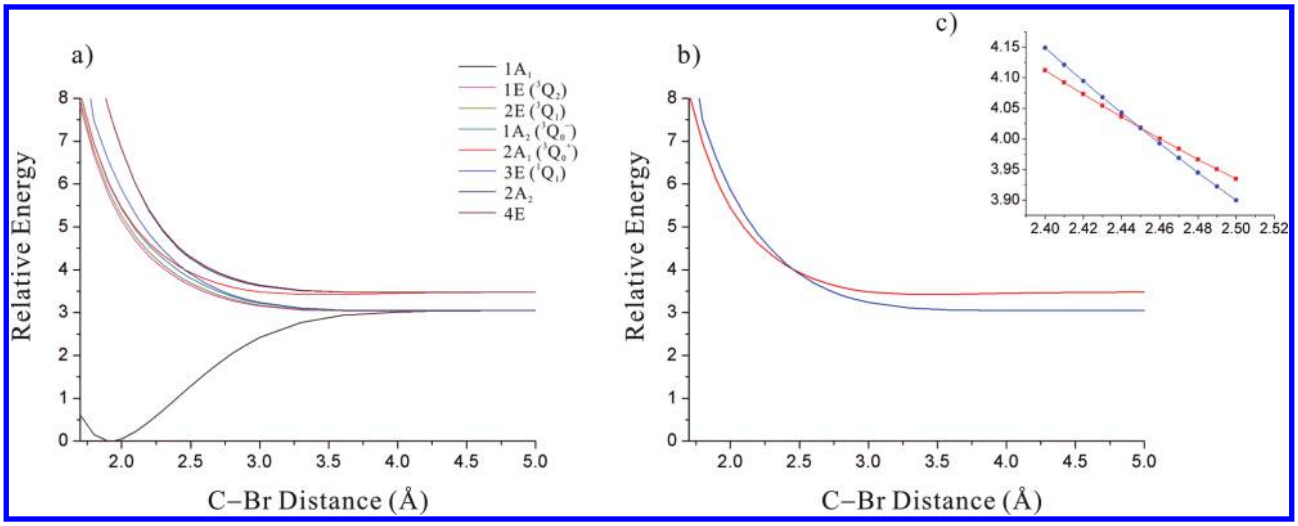

Figure 2. (a) Potential energy curves of low-lying excited states of CF_3Br calculated by SO-MCQDPT. (b) Only $2A_1$ and 3E states are shown. (c) Inset shows the region of the crossing point expanded.

(see Table 2). This result partially supports that the selection of active orbitals and the all-electron basis set is adequate for the multiconfigurational ab initio calculations. The T_v values of SO coupled states are 1E ($^3Q_2$): 5.64 eV (45 518 cm^{-1}); 2E ($^3Q_1$): 5.75 eV (46 393 cm^{-1}); $1A_2$ ($^3Q_0^-$): 5.92 eV (47 727 cm^{-1}); $2A_1$ ($^3Q_0^+$): 5.94 eV (47 931 cm^{-1}); 3E ($^1Q_1$): 6.43 eV (51 868 cm^{-1}); $2A_2$: 7.60 eV (61 268 cm^{-1}); and 4E: 7.60 eV (61 316 cm^{-1}), in order of ascending energy. Two SO states (Br*($^2P_{1/2}$) and Br($^2P_{3/2}$)) are generated due to SOC in the dissociation limit along the C—Br coordinate. The energy difference between Br* ($^2P_{1/2}$) and Br ($^2P_{3/2}$) states calculated by SO-MCQDPT is 0.43 eV, in good agreement with the experimental value (0.46 eV).[52] All of the excited-state PECs are repulsive curves, and the states' electronic curve crossing leading to two different dissociation channels (Br* and Br) is seen. The region of curve crossing is magnified in Figure 2c. The crossing point between the 3E ($^1Q_1$) and $2A_1$ ($^3Q_0^+$) states is located near 2.45 Å, almost identical to that of CH_3Br (near 2.45 Å) and is slightly longer than those of CF_3I (near 2.372 Å) and CH_3I (near 2.374 Å) calculated by RASSI-SO.[2] This result suggests that the locations of the crossing points are not altered by fluorination.

Photofragment ion-imaging studies of CF_3Br at 234[13] and 225 nm[12] suggest that excited Br*($^2P_{1/2}$) atoms are mainly produced through a direct dissociation pathway from the initial excitation to the only $2A_1$ ($^3Q_0^+$) state. For CF_3I, by contrast, ground-state iodine atoms are mainly generated from the curve-crossing pathway at 277 nm, where there is an initial excitation to the $^3Q_0^+$ state and curve crossing to the $^1Q_1$ state.[53] The Landau–Zener model[54] can be used to explain the difference in curve-crossing probability (P) between CF_3Br and CF_3I at the wavelength in which the $^3Q_0^+$ state is exclusively populated

$$P = 1 - \exp\left(-\frac{2\pi|V_{ij}|^2}{\hbar v_c|\Delta F_{ij}|}\right) \quad (1)$$

where V_{ij} is the coupling term between diabatic potentials (in this case the $^3Q_0^+$ and $^1Q_1$ states), ΔF_{ij} the gradient difference between two PECs at the crossing point, and v_c the effective velocity through the crossing point. Unfortunately, V_{ij} cannot be quantitatively stated because a program that can calculate the nonadiabatic coupling matrix element for two SO coupled states is not currently available. In addition, because previous theoretical study showed only PECs, PECs did not fit into analytical functions such as exponential functions. Therefore, information of ΔF_{ij} for other halomethanes' PECs is limited (CH_3Br, CH_3I, and CF_3I).[2] Therefore, crossing probability can only be discussed in terms of the effective velocity. Potential energy differences in the $2A_1$ ($^3Q_0^+$) state between at the ground-state equilibrium geometry (2.150 Å for CF_3I and 1.920 Å for CF_3Br) and at the crossing point (2.372 Å for CF_3I and 2.450 Å for CF_3Br) are ~7887 cm^{-1} for CF_3I (see Table 4 of ref 2) and 15 522 cm^{-1} (= 47 931 − 32 409 at the SO-MCQDPT level) for CF_3Br. This indicates that CF_3Br has larger kinetic energy than CF_3I, and thus, CF_3Br has much larger velocity than CF_3I. Landau–Zener theory suggests that higher velocity reduces crossing probability, and thus, the calculated $2A_1$ ($^3Q_0^+$) PEC and the crossing point for CF_3Br predicts preference for direct dissociation (Br*, $^2P_{1/2}$ state). Although comprehensive conclusions cannot be made because only one factor has been considered for the crossing probability, this prediction may be related to recent experimental findings for CF_3Br; after 225 nm irradiation, where only the $2A_1$ ($^3Q_0^+$) state is active, 95% of the direct dissociation channel is populated.[12] Finally, the BDE (D_e) calculated by SO-MCQDPT is 3.05 eV (70.4 kcal/mol). It agrees with the upper limit of the corresponding experimental value of D_0 (70.1 ± 0.3 kcal/mol). In summary, SO-MCQDPT gives a good description of SOC and a reasonable estimation of BDE.

4. CONCLUSIONS

Molecular structure and vibrational frequencies of the CF_3 radical and CF_3Br and the dipole moment, the BDE of the C—Br bond, and T_v values of CF_3Br are calculated by various DFT, TDDFT, and ab initio methods. The performances of six hybrid and five hybrid meta functionals are assessed. Unfortunately, no DFT functional gives good results for all molecular properties simultaneously. The ωB97X functional provides excellent results for the molecular structure of CF_3Br. In particular, it calculates molecular structure in excellent agreement with CCSD(T). The ωB97X functional is therefore recommended for calculating the molecular structures of halomethanes and haloethanes. B3PW91 provides very good estimations of the vibrational frequencies of CF_3Br, whereas the hybrid meta functional generally overestimates

them. The ωB97X functional calculates the dipole moment well. The BDE calculated by M05-2X is in excellent agreement with experimental result. All TDDFT methods give red-shifted T_v values compared with those of EOM-CCSD. Among the DFT methods, the M05-2X functional gives closer results to those of EOM-CCSD, and thus, M05-2X is the best choice for TDDFT calculations. In addition, B3LYP and TPSSh should not be used to calculate the molecular properties of halomethanes and haloethanes.

Photodissociation of CF_3Br is investigated using the multiconfigurational SO ab initio method. Twelve SO coupled states of CF_3Br are generated. The energy difference between $Br^*(^2P_{1/2})$ and Br $(^2P_{3/2})$ states calculated by SO-MCQDPT is 0.43 eV, in good agreement with the experimental value. The curve crossing point is found to be near the C—Br bond length of 2.45 Å, the same as that for CH_3Br and longer than those of CH_3I and CF_3I. These results indicate that fluorination does not alter the location of crossing point. Consideration of the calculated PECs and crossing points for CF_3Br on the basis of Landau−Zener theory predicts preference for direct dissociation, which may be related to the recent experimental results. SO-MCQDPT provides relevant PECs including SOC. This work could aid further experimental and theoretical investigation of halomethanes and haloethanes.

■ ASSOCIATED CONTENT

Supporting Information. Methods' performances for various molecular properties are summarized in Table S1. The active orbitals of CF_3Br for CAS(6,6) calculations are depicted in Figure S1. The scatter plot of the percentage error of the C—Br bond length (*x*-axis) versus the MAE of T_v values (*y*-axis) is depicted in Figure S2. This material is available free of charge via the Internet at http://pubs.acs.org.

■ AUTHOR INFORMATION

Corresponding Author

*E-mail: hyotcherl.ihee@kaist.ac.kr (H.I.); tkkim@pusan.ac.kr (T.K.K.).

■ ACKNOWLEDGMENT

We thank Mr. Jong Hyuk Lee for his assistance and Prof. Yoon Sup Lee for helpful discussions. This work was supported by the Creative Research Initiatives (Center for Time-Resolved Diffraction) of MEST/NRF. We acknowledge the support from the WCU program.

■ REFERENCES

(1) Ajitha, D.; Fedorov, D. G.; Finley, J. P.; Hirao, K. *J. Chem. Phys.* **2002**, *117*, 7068.
(2) Ajitha, D.; Wierzbowska, M.; Lindh, R.; Malmqvist, P. A. *J. Chem. Phys.* **2004**, *121*, 5761.
(3) Alekseyev, A. B.; Liebermann, H. P.; Buenker, R. J. *J. Chem. Phys.* **2007**, *126*, 234102.
(4) Alekseyev, A. B.; Liebermann, H. P.; Buenker, R. J. *J. Chem. Phys.* **2007**, *126*, 234103.
(5) Amatatsu, Y.; Yabushita, S.; Morokuma, K. *J. Chem. Phys.* **1996**, *104*, 9783.
(6) Kim, J.; Jun, S.; Kim, J.; Ihee, H. *J. Phys. Chem. A* **2009**, *113*, 11059.
(7) Yabushita, S.; Morokuma, K. *Chem. Phys. Lett.* **1988**, *153*, 517.
(8) de Nalda, R.; Izquierdo, J. G.; Dura, J.; Bañares, L. *J. Chem. Phys.* **2007**, *126*, 021101.
(9) Dura, J.; de Nalda, R.; Alvarez, J.; Izquierdo, J. G.; Amaral, G. A.; Bañares, L. *ChemPhysChem* **2008**, *9*, 1245.
(10) Ihee, H.; Lobastov, V. A.; Gomez, U. M.; Goodson, B. M.; Srinivasan, R.; Ruan, C. Y.; Zewail, A. H. *Science* **2001**, *291*, 458.
(11) Ihee, H.; Lorenc, M.; Kim, T. K.; Kong, Q. Y.; Cammarata, M.; Lee, J. H.; Bratos, S.; Wulff, M. *Science* **2005**, *309*, 1223.
(12) Kim, T. K.; Lee, K. W.; Lee, K. S.; Lee, E. K.; Jung, K. H. *Chem. Phys. Lett.* **2007**, *446*, 31.
(13) Kim, T. K.; Park, M. S.; Lee, K. W.; Jung, K. H. *J. Chem. Phys.* **2001**, *115*, 10745.
(14) Lee, J. H.; Kim, J.; Cammarata, M.; Kong, Q.; Kim, K. H.; Choi, J.; Kim, T. K.; Wulff, M.; Ihee, H. *Angew. Chem., Int. Ed.* **2008**, *47*, 1047.
(15) Lee, J. H.; Kim, T. K.; Kim, J.; Kong, Q.; Cammarata, M.; Lorenc, M.; Wulff, M.; Ihee, H. *J. Am. Chem. Soc.* **2008**, *130*, 5834.
(16) Li, G. S.; Shin, Y. K.; Hwang, H. J. *J. Phys. Chem. A* **2005**, *109*, 9226.
(17) Rubio-Lago, L.; Garcia-Vela, A.; Arregui, A.; Amaral, G. A.; Bañares, L. *J. Chem. Phys.* **2009**, *131*, 174309.
(18) Thelen, M. A.; Felder, P. *Chem. Phys.* **1996**, *204*, 135.
(19) Underwood, J. G.; Powis, I. *Phys. Chem. Phys. Chem.* **2000**, *2*, 747.
(20) Becke, A. D. *Phys. Rev. A* **1988**, *38*, 3098.
(21) Lee, C.; Yang, W.; Parr, R. G. *Phys. Rev. B* **1988**, *37*, 785.
(22) Becke, A. D. *J. Chem. Phys.* **1993**, *98*, 5648.
(23) Adamo, C.; Barone, V. *J. Chem. Phys.* **1999**, *110*, 6158.
(24) Adamo, C.; Barone, V. *J. Chem. Phys.* **1998**, *108*, 664.
(25) Perdew, J. P. *Electronic Structure of Solids*; Akademic Verlag: Berlin, Germany, 1991.
(26) Wilson, P. J.; Bradley, T. J.; Tozer, D. J. *J. Chem. Phys.* **2001**, *115*, 9233.
(27) Chai, J. D.; Head-Gordon, M. *J. Chem. Phys.* **2008**, *128*, 084106.
(28) Becke, A. D. *J. Chem. Phys.* **1996**, *104*, 1040.
(29) Staroverov, V. N.; Scuseria, G. E.; Tao, J. M.; Perdew, J. P. *J. Chem. Phys.* **2003**, *119*, 12129.
(30) Boese, A. D.; Martin, J. M. L. *J. Chem. Phys.* **2004**, *121*, 3405.
(31) Zhao, Y.; Schultz, N. E.; Truhlar, D. G. *J. Chem. Theory Comput.* **2006**, *2*, 364.
(32) Zhao, Y.; Truhlar, D. G. *Theor. Chem. Acc.* **2008**, *120*, 215.
(33) Frisch, M. J.; Head-Gordon, M.; Pople, J. A. *Chem. Phys. Lett.* **1990**, *166*, 281.
(34) Head-Gordon, M.; Head-Gordon, T. *Chem. Phys. Lett.* **1994**, *220*, 122.
(35) Raghavachari, K.; Trucks, G. W.; Pople, J. A.; Head-Gordon, M. *Chem. Phys. Lett.* **1989**, *157*, 479.
(36) Peterson, K. A.; Figgen, D.; Goll, E.; Stoll, H.; Dolg, M. *J. Chem. Phys.* **2003**, *119*, 11113.
(37) Bauernschmitt, R.; Ahlrichs, R. *Chem. Phys. Lett.* **1996**, *256*, 454.
(38) Hirata, S.; Head-Gordon, M. *Chem. Phys. Lett.* **1999**, *302*, 375.
(39) Hirata, S.; Head-Gordon, M. *Chem. Phys. Lett.* **1999**, *314*, 291.
(40) Foresman, J. B.; Headgordon, M.; Pople, J. A.; Frisch, M. J. *J. Phys. Chem.* **1992**, *96*, 135.
(41) Kallay, M.; Gauss, J. *J. Chem. Phys.* **2004**, *121*, 9257.
(42) Boys, S. F.; Bernardi, F. *Mol. Phys.* **1970**, *19*, 553.
(43) Frisch, M. J.; Trucks, G. W.; Schlegel, H. B.; Scuseria, G. E.; Robb, M. A.; Cheeseman, J. R.; Scalmani, G.; Barone, V.; Mennucci, B.; Petersson, G. A.; Nakatsuji, H.; Caricato, M.; Li, X.; Hratchian, H. P.; Izmaylov, A. F.; Bloino, J.; Zheng, G.; Sonnenberg, J. L.; Hada, M.; Ehara, M.; Toyota, K.; Fukuda, R.; Hasegawa, J.; Ishida, M.; Nakajima, T.; Honda, Y.; Kitao, O.; Nakai, H.; Vreven, T.; Montgomery, Jr., J. A.; Peralta, J. E.; Ogliaro, F.; Bearpark, M.; Heyd, J. J.; Brothers, E.; Kudin, K. N.; Staroverov, V. N.; Kobayashi, R.; Normand, J.; Raghavachari, K.; Rendell, A.; Burant, J. C.; Iyengar, S. S.; Tomasi, J.; Cossi, M.; Rega, N.; Millam, N. J.; Klene, M.; Knox, J. E.; Cross, J. B.; Bakken, V.; Adamo, C.; Jaramillo, J.; Gomperts, R.; Stratmann, R. E.; Yazyev, O.; Austin, A. J.; Cammi, R.; Pomelli, C.; Ochterski, J. W.; Martin, R. L.; Morokuma, K.; Zakrzewski, V. G.; Voth, G. A.; Salvador, P.; Dannenberg, J. J.; Dapprich,

S.; Daniels, A. D.; Farkas, Ö.; Foresman, J. B.; Ortiz, J. V.; Cioslowski, J.; Fox, D. J. *Gaussian 09*, revision A.1; Gaussian, Inc.: Wallingford CT, 2009.

(44) Roos, B. O. *Advances in Chemical Physics; Ab Initio Methods in Quantum Chemistry II*; John Wiley and Sons: Chichester, England, 1987.

(45) Hess, B. A. *Phys. Rev. A* **1986**, *33*, 3742.

(46) Jansen, G.; Hess, B. A. *Phys. Rev. A* **1989**, *39*, 6016.

(47) Fedorov, D. G.; Finley, J. P. *Phys. Rev. A* **2001**, *64*, 042502.

(48) Schmidt, M. W.; Baldridge, K. K.; Boatz, J. A.; Elbert, S. T.; Gordon, M. S.; Jensen, J. H.; Koseki, S.; Matsunaga, N.; Nguyen, K. A.; Su, S. J.; Windus, T. L.; Dupuis, M.; Montgomery, J. A. *J. Comput. Chem.* **1993**, *14*, 1347.

(49) Ihee, H.; Kua, J.; Goddard, W. A.; Zewail, A. H. *J. Phys. Chem. A* **2001**, *105*, 3623.

(50) Delvalle, F. J. O.; Tolosa, S.; Ojalvo, E. A.; Espinosa, J. *Chem. Phys.* **1988**, *127*, 343.

(51) Kim, J.; Lee, H. M.; Suh, S. B.; Majumdar, D.; Kim, K. S. *J. Chem. Phys.* **2000**, *113*, 5259.

(52) Husain, D.; Donovan, R. J. *J. Adv. Photochem.* **1971**, *8*, 1.

(53) Kim, Y. S.; Kang, W. K.; Jung, K. H. *J. Chem. Phys.* **1996**, *105*, 551.

(54) Nakamura, H. *J. Chem. Phys.* **1987**, *87*, 4031.

(55) Yamada, C.; Hirota, E. *J. Chem. Phys.* **1983**, *78*, 1703.

(56) Lide, D. R. *CRC Handbook of Chemistry and Physics*, 88th ed.; CRC Press: Boca Raton, FL, 2008.

(57) Cox, A. P.; Duxbury, G.; Hardy, J. A.; Kawashima, Y. *J. Chem. Soc., Faraday Trans. 2* **1980**, *76*, 339.

(58) Polo, S. R.; Wilson, M. K. *J. Chem. Phys.* **1952**, *20*, 1183.

(59) Doucet, J.; Sauvageau, P.; Sandorfy, C. *J. Chem. Phys.* **1973**, *58*, 3708.

(60) Asher, R. L.; Ruscic, B. *J. Chem. Phys.* **1997**, *106*, 210.